EFFICIENT LARGE EDDY SIMULATION OF A LOW-MACH NUMBER AXIAL FAN

Sergei G. CHUMAKOV[1], Sanjeeb T. BOSE[2], Frank E. HAM[2]

[1] *Research and Technology Center, Robert Bosch LLC, 4005 Miranda Ave, Palo Alto, CA 94304, U.S.A.*

[2] *Cascade Technologies Inc., 2445 Faber Pl., Palo Alto, CA 94303, U.S.A.*

SUMMARY

A weakly-compressible formulation for Large Eddy Simulation (LES) is shown to be a suitable tool for simulation of fan flow as a part of a fan noise prediction effort. LES can directly capture the inertial-range turbulence that produces the broadband component of the noise. In the present formulation, the density and pressure are coupled in each time step through an isentropic relationship. When solved using a fractional-step method, this density-pressure coupling leads to a Helmholtz system for pressure that implicitly captures the acoustics without introducing additional numerical stiffness. The method is applied to an experimental configuration and shows good agreement with both integral parameters and flow velocity statistics.

INTRODUCTION

The traditional approach to industrial fan design has historically been using empirical trial-and-error methods based on rapid prototyping, expert knowledge and intuition. However, in current environment the development of new design concepts must rely on methods that are able to account for three-dimensional unsteady flow patterns. A notable increase in importance of aero-acoustic performance of new fans means that the design tools should be able to predict not just the time-averaged flow but also turbulent intermittency which is generally responsible for the broadband component of the flow-borne noise. By developing virtual prototypes one can identify potential design problems and solutions to these at early stages of the design process thus reducing the development costs. This can be one of the reasons for the observed increase in CFD effort in industry.

In turbomachinery and fan design, Reynolds-averaged Navier-Stokes (RANS) and unsteady RANS (URANS) are well-established methods that are able to predict time- or ensemble-averaged quantities. However, prediction of intermittency-related phenomena such as noise is extremely challenging with these methods. A significant improvement can be achieved if URANS is paired with Large Eddy Simulation (LES), a method that computes locally-averaged flow quantities. LES is able to account for unsteady flow effects with high accuracy, albeit at higher cost. Coupling LES and RANS can be used to capture at least part of the unsteadiness of the flow [1].

At the moment, attempts to run a full-scale LES of turbomachinery appear scarce in the open literature (e.g., [2-4]). Due to significant computational cost if compared to RANS, LES is usually

reserved for parts of components [5,6], small domains, or to gain a physical insight into a particular unsteady phenomena, e.g., trailing-edge airfoil noise [7,8]. However, sustained advancements in the area of High-Performance Computing (HPC) are making it possible to incorporate LES in the product development process in the near future.

The present work focuses on an LES simulation of a flow through a free-tip automotive cooling fan. We utilize the code VIDA from Cascade Technologies, which solves a weakly compressible version of the Navier-Stokes equations in the rotating reference frame. The density perturbations are assumed to be isentropic which leads to solution of Helmholtz system for pressure, which in turn leads to a significant speedup in the run-time when compared to a fully incompressible LES. The results are validated by means of comparison with state-of-the-art PIV measurements in the fan wake.

APPROACH AND IMPLEMENTATION

The LES code VIDA solves the spatially-filtered Navier-Stokes equations on unstructured grids using a mixed finite volume / finite element discretization [9]. The unknowns are stored at the nodes of a general unstructured grid, with dual volumes constructed around each node using the median-dual approach – see Figure 1.

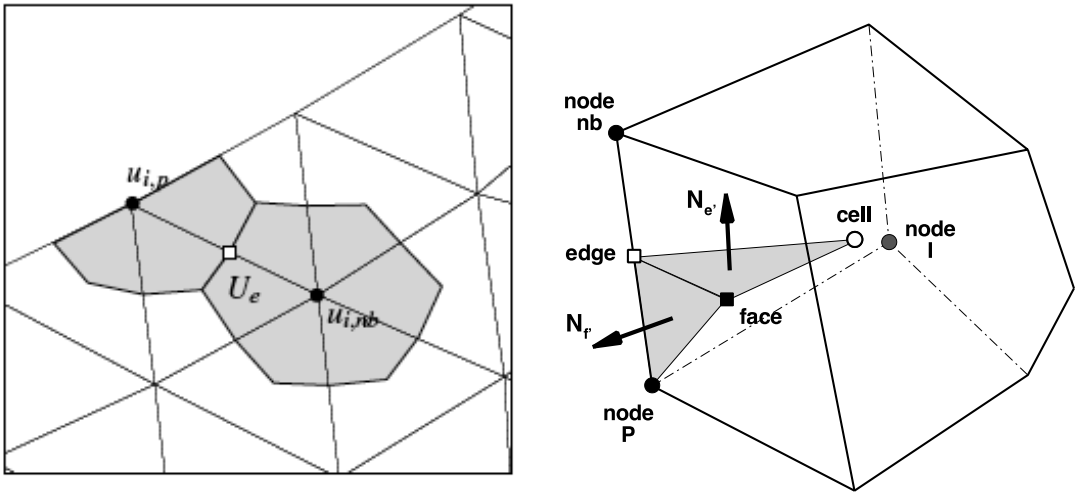

Figure 1: Schematic of dual formulation showing location of velocity, pressure and density at the nodes (including along boundaries), and face-based normal momentum components. In 3D (right), the fluxes between nodes are evaluated for each internal triangle made up of edge-face-cell centers ($N_{e'}$), and for each boundary triangle made up of node-edge-face centers ($N_{f'}$).

To minimize the numerical dissipation in the solver while still maintaining numerical stability, the spatial discretization of convective terms uses a mixture of a central difference scheme and a third-order upwind scheme, where the relative fraction of the upwind scheme is computed locally based on the lack of skew-symmetry in the central differencing operator [10]. In this way, in regions of very high quality Cartesian meshes, where the differencing operator is skew-symmetric, there will be no numerical dissipation resulting from the convective discretization. Viscous terms, including the molecular viscosity and sub-grid eddy-viscosity from the sub-grid model are discretized using a linear finite element method.

The time discretization is now described in some detail, as it is the particularly unique aspect of the solver. Due to the collocated nature of the formulation, the discrete continuity equation is enforced on a velocity field interpolated to the flux triangle locations at the edges ($N_{e'}$ in Figure 1). In each time step, the algorithm proceeds as follows:

1. Predict the edge-based momentum to the new time level using Adams-Bashforth extrapolation from the previous 2 time levels.
2. Solve a Helmholtz system for pressure and correct the edge-based momentum and node based density to discretely satisfy continuity at the new time level. In the Helmholtz system, pressure and density are linked using the isentropic relation $\rho' = p'/c^2$, where c is the (prescribed constant) sound speed in the simulation. As a result, instead of the Poisson equation, the pressure p is computed as solution to the Helmholtz equation:
$$-\frac{1}{(c\,\Delta t)^2}p' + DGp' = \frac{1}{\Delta t}D(\rho u)^*$$
Here, D is the discrete divergence operator, c is the speed of sound, G is the discrete gradient operator, $(\rho u)^*$ is the predicted momentum at the edges, and p' is the fluctuating component of the pressure.
3. Solve the linearized momentum equation using the frozen edge-based momentum and node-based density field computed in the previous step. This step includes the pressure gradient term based on the pressure from the previous time step.
4. Finally, solve a second Helmholtz system for pressure, and correct both edge-based momentum and node-based density fields, once again assuming an isentropic relation between pressure and density.

In all present cases, sub-grid scale turbulence fluctuations were modeled using the Vreman model [11]. Unlike simpler closures such as the Smagorinsky model [12,13], the Vreman model behaves reasonably well near resolved walls, effectively switching off and properly predicting the wall shear stress.

To verify the expected 2nd-order accuracy for both flow and acoustics, an isentropic Euler vortex was computed [14]. The Euler vortex is an exact solution to the compressible Euler equations. Figure 2 shows the convergence of the method with grid refinement, confirming the second-order behavior.

A significant advantage of the Helmholtz system is its improved condition number relative to the Poisson system, making it faster to solve in each time step, and improving scalability, particularly for very large-scale simulations where the Poisson solver becomes a critical bottleneck. Overall, VIDA running with the Helmholtz pressure equation is about 30% faster than the fully incompressible VIDA running with the Poisson pressure equation.

ENGINE COOLING FAN SIMULATION

Domain configuration and simulation parameters

The schematic of the LES domain configuration is given in the Figure 3. The computational domain was chosen to correspond to the experimental setup for the PIV measurements that were used to validate LES [15] as well as to a setup in Bosch anechoic chamber where the acoustic measurements were taken [16]. The domain consists of upstream and downstream sections of a circular pipe with fan and shroud in the middle. The pipe diameter is 0.7m, both upstream and downstream sections are roughly 1m in length, and the fan diameter is set to 0.32m. The significance of the upstream side extent of the duct was strategically different between each setup – for the LES computation domain and the PIV facility, the upstream duct was primarily a mean to provide controlled inflow condition for the fan. For the LES computation domain, the space is also used to attenuate the reflection of acoustic waves at the numerical boundary. This was done via utilization of a numerical sponge upstream of the fan, in which a numerical scheme with high numerical dissipation was used (a classic Godunov scheme with piecewise-linear face reconstruction algorithm [17]. The downstream section of the pipe terminates with an outlet of diameter of 16 cm.

For simulation and measurements, the rotational speed was equal to 2630 min^{-1}, the volumetric flow rate was fixed at 0.53 m^3/s, which in experiments resulted in the pressure rise of approximately 75 Pa across the fan (referred to as "operating point 2", or OP2). The operating point OP2, along with the fan performance curve is shown in the Figure 4. This particular operating point was chosen for the LES validation due to availability of experimental data for both flow and noise and also due to the apparent absence of any natural unsteadiness in the flow such as rotating stall.

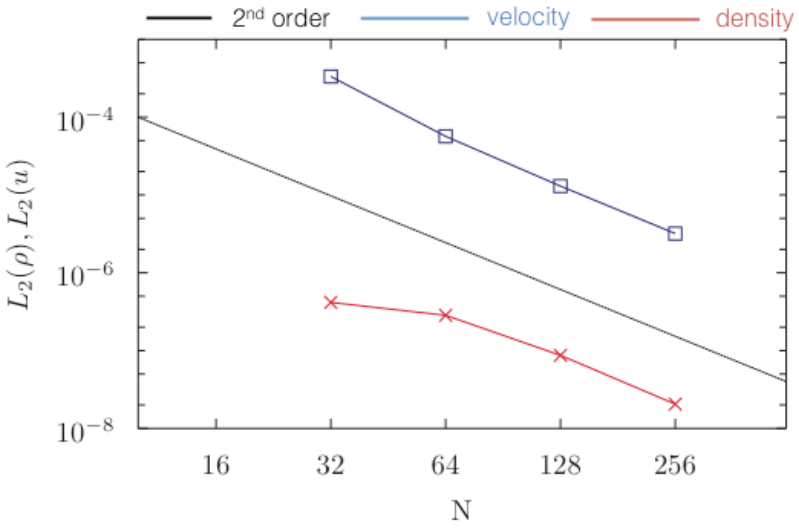

Figure 2: Reduction in L^2-error for density and velocity with grid refinement, compressible isentropic Euler vortex test case.

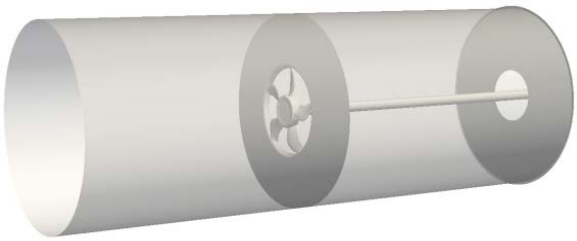

Figure 3: Schematic of the computational domain.

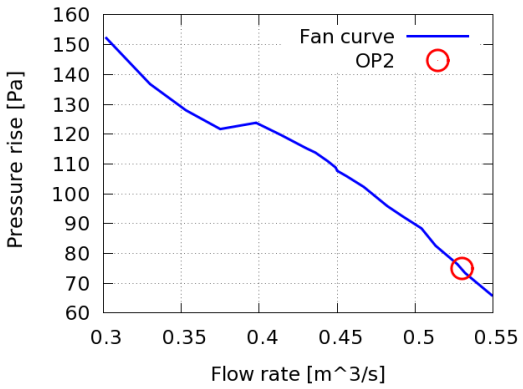

Figure 4: Fan performance curve and operating point OP2.

As the inlet boundary conditions, a prescribed mass flow rate was specified, and at the outlet ambient pressure boundary conditions were chosen. The acoustic setup in addition had a parabolic-shaped bell-mouth attached to the front end of the pipe, but LES domain terminated in a simple circular inlet, and a uniform inflow was assumed.

To reduce overall computational cost of the simulation, the "spin-up" runs were performed on a series of computational meshes with successive refinement. Once the simulation reached a steady state, as determined by the stabilization of pressure rise across the fan and the overall mass flow rate, the full simulation was ran for about 0.5 seconds (about 20 fan rotations) during which the statistics were gathered.

To take advantage of the symmetry of the domain, the computations were performed in the rotating reference frame. However, the simulation was not confined to a single blade [5] and included full domain. This was done to set up a framework for successive LES of phenomena with characteristic frequencies other than the blade passing frequency (BPF), such as rotating stall and tip vortex meandering (e.g., [1], [18-20]).

Computational mesh

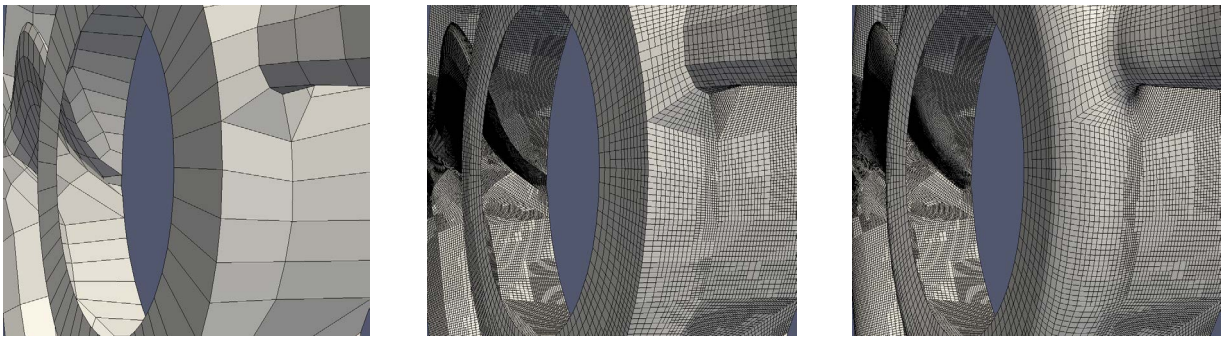

a) *b)* *c)*

Figure 5: Illustration of the ADAPT refinement and projection algorithm – refinement in the hub area of the engine cooling fan. a) Skeletal mesh; b) refined mesh without boundary projection; c) refined mesh with boundary projection.

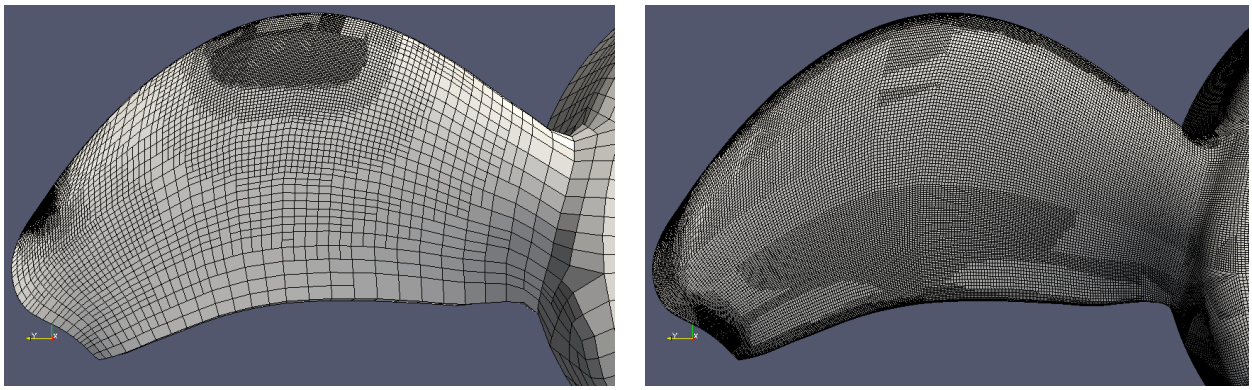

a) b)

Figure 6: Different refinement criteria: a) two refinement windows were specified with target cell dimensions; b) curvature-based refinement.

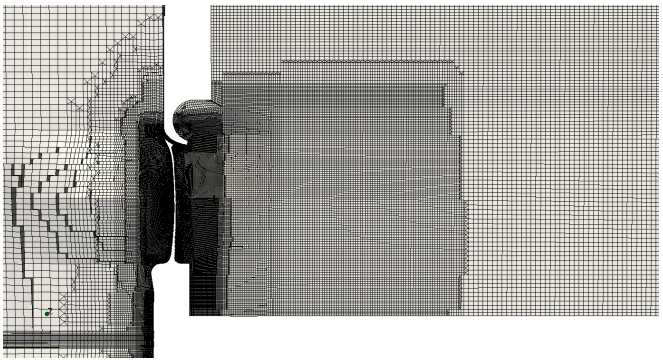

Figure 7: A slice of computational domain with mesh.

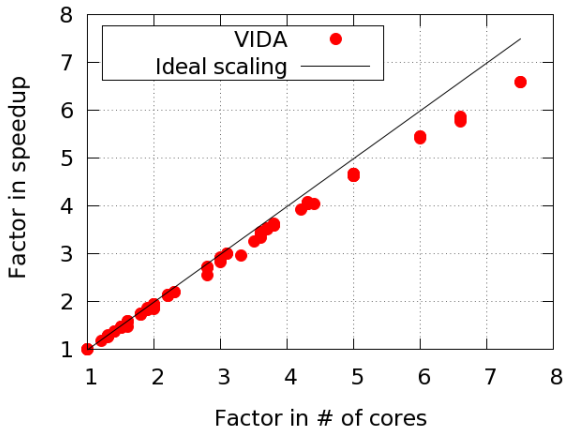

Figure 8: VIDA scaling on 47M node mesh.

The mesh generation was performed in two steps. As a first step, a very coarse ("skeletal") mesh was generated in the domain using ANSYS Mesher. During the second step, the skeletal mesh was refined by a modified ADAPT tool from Cascade Technologies[10]. The algorithm refines the

given mesh in user-specified areas and keeps the domain boundaries conformal to the surfaces that are given as a separate input. An example of this refinement is given in the Figure 5, where we show the skeletal surface mesh on the fan hub and blades, together with the refined mesh – with and without the projection.

Various mesh refinement algorithms can be employed based on different criteria, such as explicit refinement window in space, proximity to a given surface or the curvature of the given surface. Figure 6 shows the surface part of two meshes mesh around a fan blade that were refined based on two different directives: the panel a) shows the result of the window-based refinement in which the refinement region is specified explicitly together with the desired cell size, while the panel b) shows the result of the surface curvature-based refinement.

Figure 7 shows a slice of the computational domain along the fan axis with computational grid. For the engine cooling fan case, the computational mesh was generated that had 47 million cells, using successive refinement around the fan blades. The minimum linear cell size was set to 0.2 mm close to the fan blade surfaces, and the maximum cell size was close to 2 cm (near the inlet area).

RESULTS AND DISCUSSION

Flow field

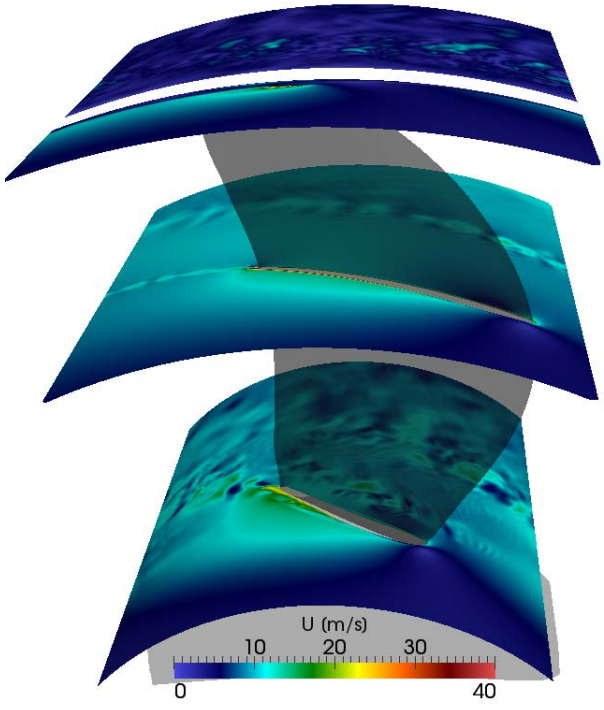

Figure 9: Velocity magnitude at three radial locations.

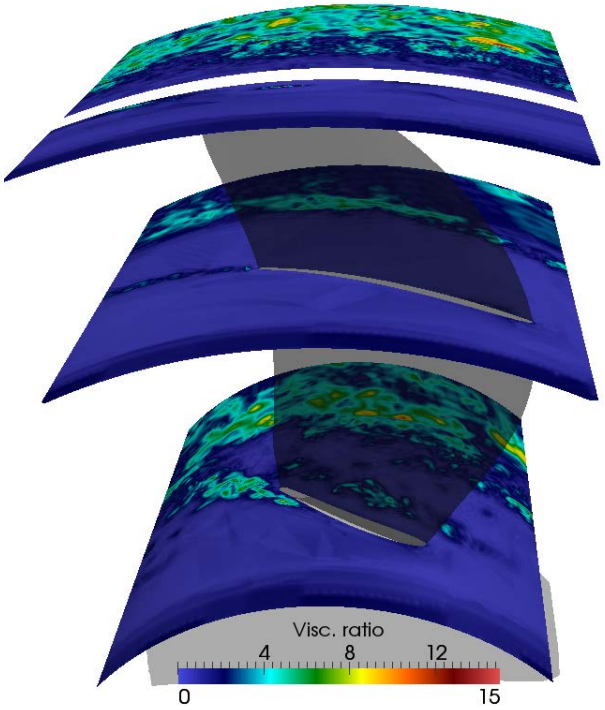

Figure 10: Ratio of subgrid to molecular viscosity at three radial locations.

The large-scale flow structures that develop around the fan blades are shown in Figures 9 and 11. The velocity (in the laboratory reference frame) is shown in the Figure 9, at three radial positions around the blade. The wake structure from the preceding blade can be clearly seen at all three radial positions. We also illustrate the complexity of the vortical structures generated by the flow by plotting the iso-surfaces of enstrophy and the parameter λ_2 for the identification of vortex lines [21-23]. To verify the degree of mesh resolution in our simulation, the ratio of subgrid to molecular

viscosity is plotted in the Figure 10. As can be seen from the Figure, the flow around the blade is well-resolved, and the effects of the SGS model are most prominent in blade wakes and further downstream. Pressure contours on the blade surface (Figure 11c) show that the simulation captures the streaks, developing hairpin vortices and separation zones on the fan blade, which results in good prediction for the shaft torque. Note that we did not use any wall models in our LES, but in subsequent work an LES wall model will be introduced.

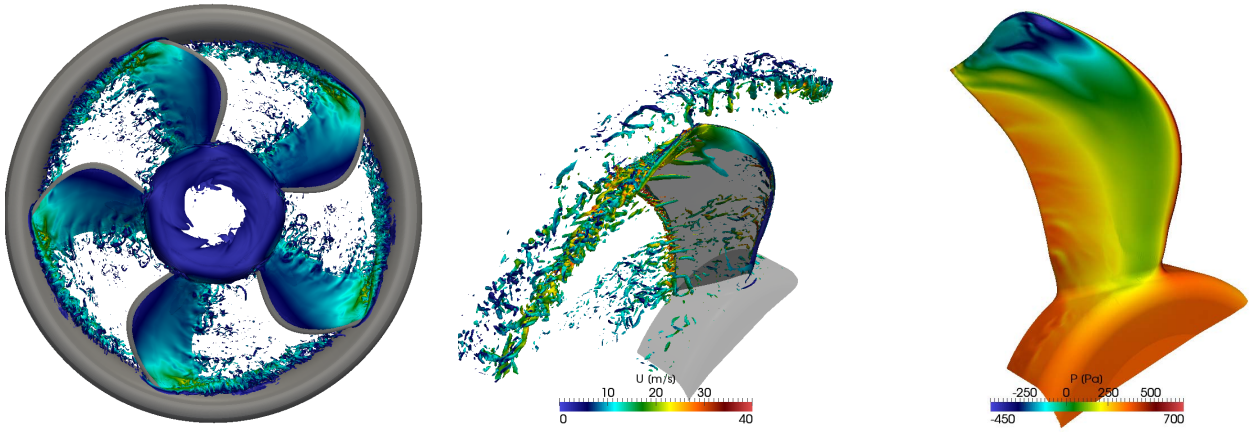

a) *b)* *c)*

Figure 11: a) Isosurface of constant enstrophy (ω^2=2.25e+6) colored by the velocity magnitude; b) Vortex identification using λ_2-criterion; c) Pressure contours on fan blade surface.

Computational cost and code scaling

The computational cost of the simulation was approximately 12,000 CPU-hours per single fan revolution. It should be mentioned that the production run was performed with the time step (dt=1e-6 s) that was much smaller than the optimal, due to the high sampling rate for the purpose of gathering acoustic data that matched the sampling rate of the acoustic measurements in the anechoic chamber. The maximum CFL number in the computational domain was observed to be close to 1.5. Because VIDA utilizes implicit time stepping, the time step could be much larger, thus reducing the needed computational time.

The code exhibits good parallel scaling, which is shown in the Figure 8. As can be seen, the speedup exponent appears to be close to linear. The scaling study was performed for the number of computational cores between 120 and 900 during the production run, which included the I/O time as well as the time spent on gathering and writing on-the-fly statistics, such as averaged quantities and their standard deviations at arrays of probe points.

Experimental data

The validation of the flow solver was performed using combination of experimental data from several sources. The velocity data from LES was compared to Particle Image Velocimetry (PIV) measurements performed at Johns Hopkins University [15], and the gross parameters (pressure rise and shaft torque) were measured at Bosch fan development facility in Waltham MA [16].

In the PIV experiment, a sodium iodide solution was used as a liquid, the fan prototype was manufactured from clear plastic and the refraction indices of the fluid and fan were matched, which allowed for optical access to virtually any location in the flow. Spatial dimensions of the experimental facility, the noise measurement facility and the LES simulation were set to be the

same. In the PIV experiment, the fan rotation rate was chosen to match the Reynolds number the flow in LES simulation. For more details on the experimental setup and technique, see [15].

Figure 12 shows the PIV measurement area, which consists of nine measurement windows. The measurements were phase-locked, with ten phases being uniformly distributed between adjacent fan blades. The phases were named P0 through P9, and as a reference, the phase P1 was chosen so that it intersects the forward-most point of the fan blade tip (see Figure 13).

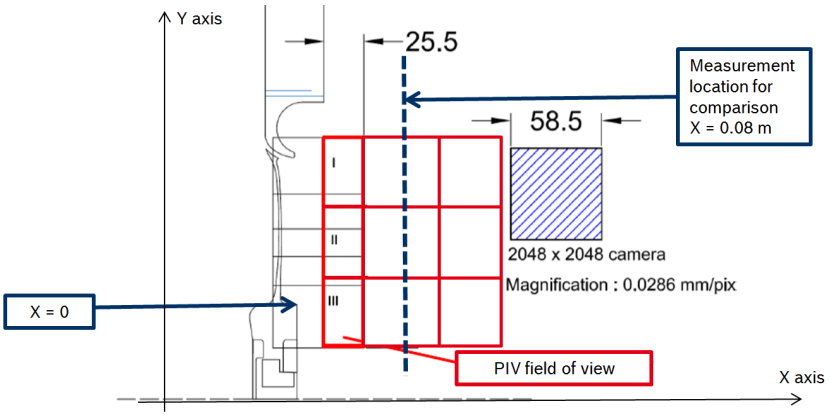

Figure 12: Location of PIV windows.

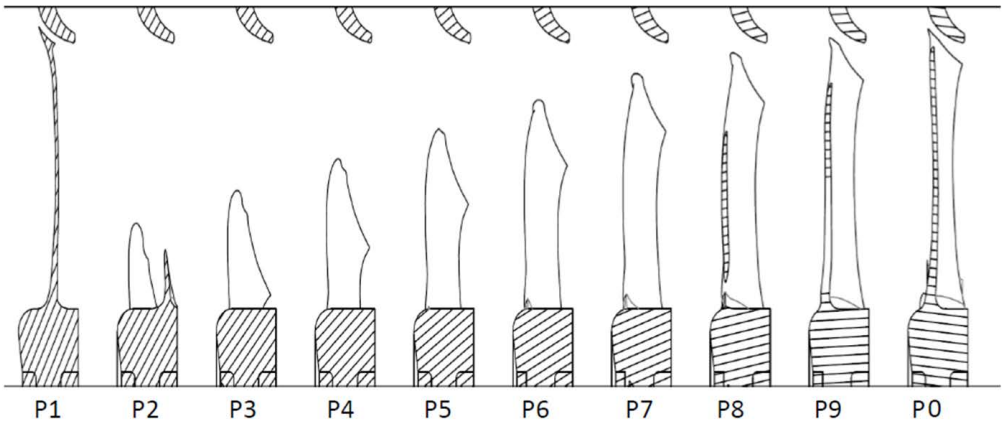

Figure 13: PIV phases. Intersection of the fan and the measurement plane are shown as shaded areas.

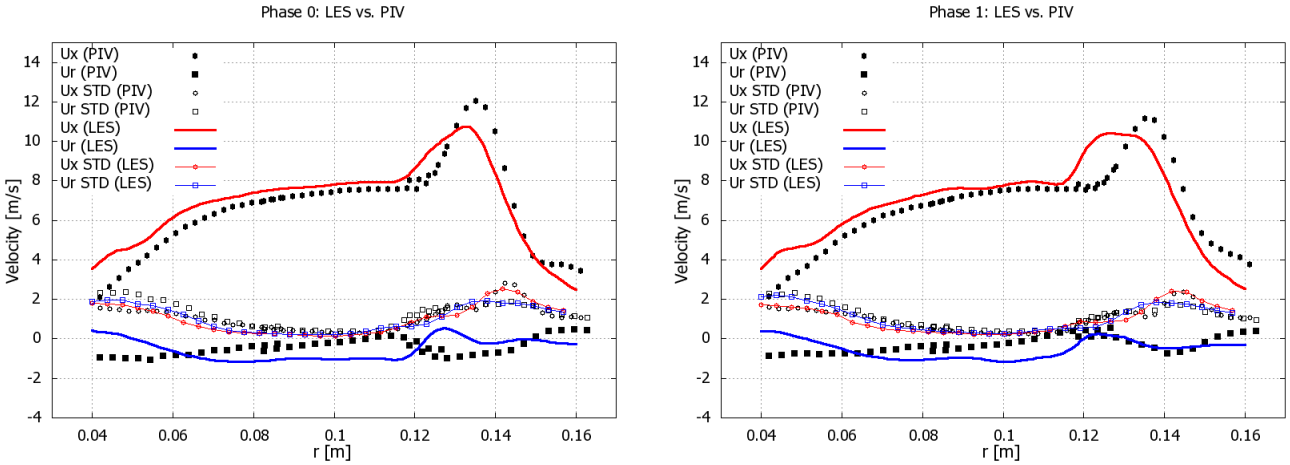

Figure 14: Comparison between LES and experimental measurements for phases 0 and 1.

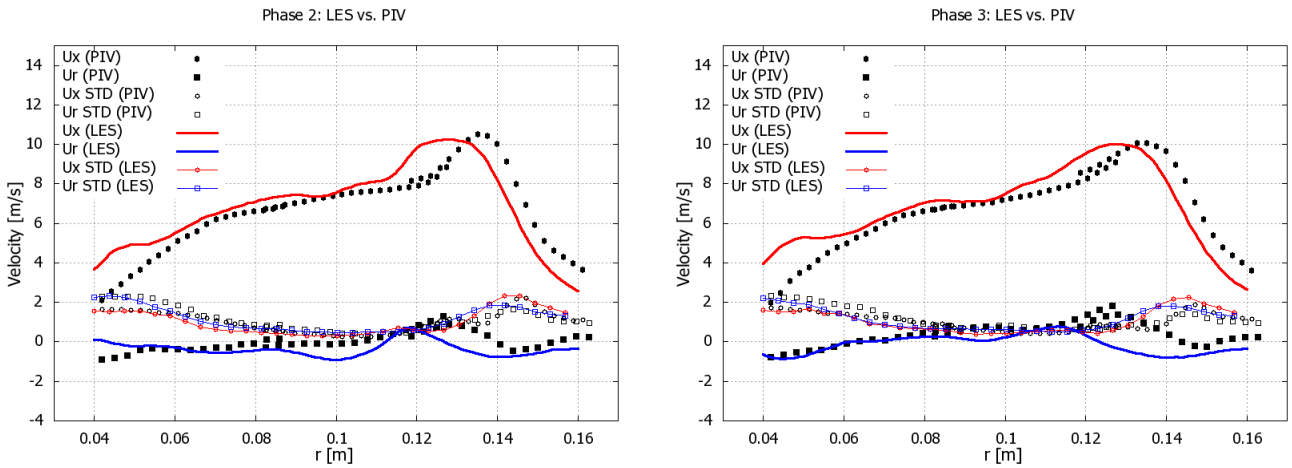

Figure 15: Comparison between LES and experimental measurements for phases 2 and 3.

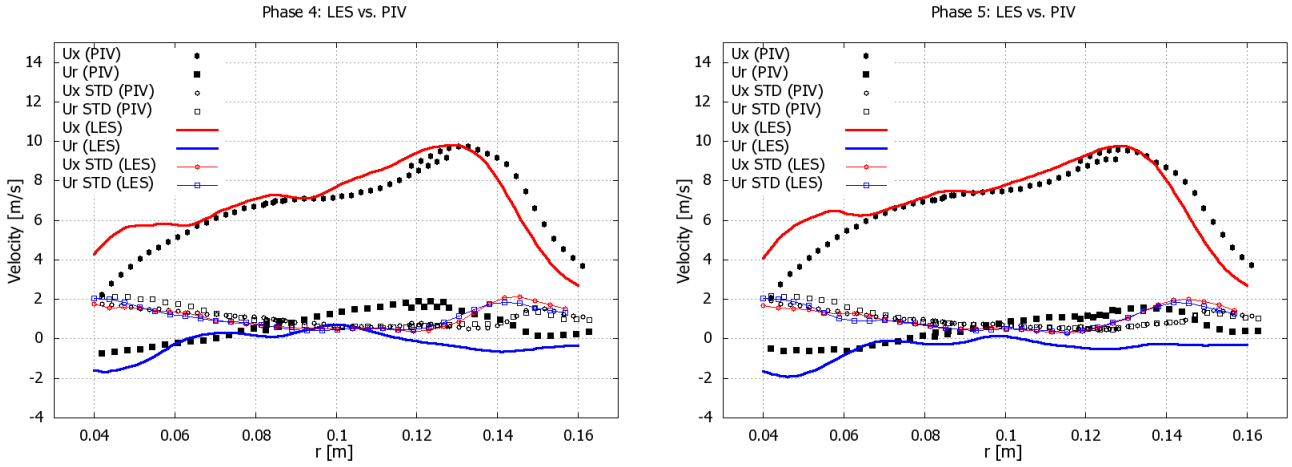

Figure 16: Comparison between LES and experimental measurements for phases 4 and 5.

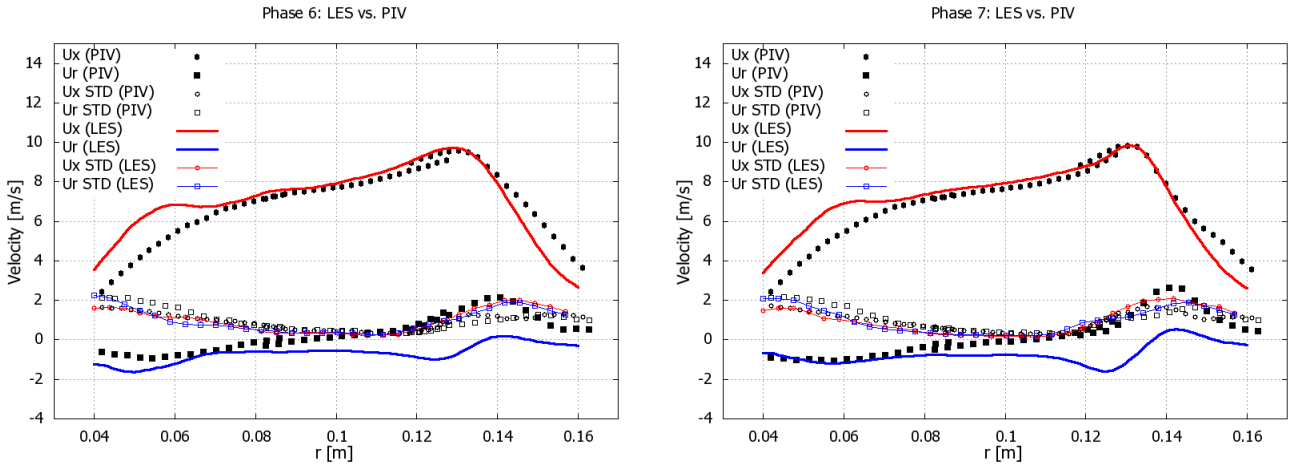

Figure 17: Comparison between LES and experimental measurements for phases 6 and 7.

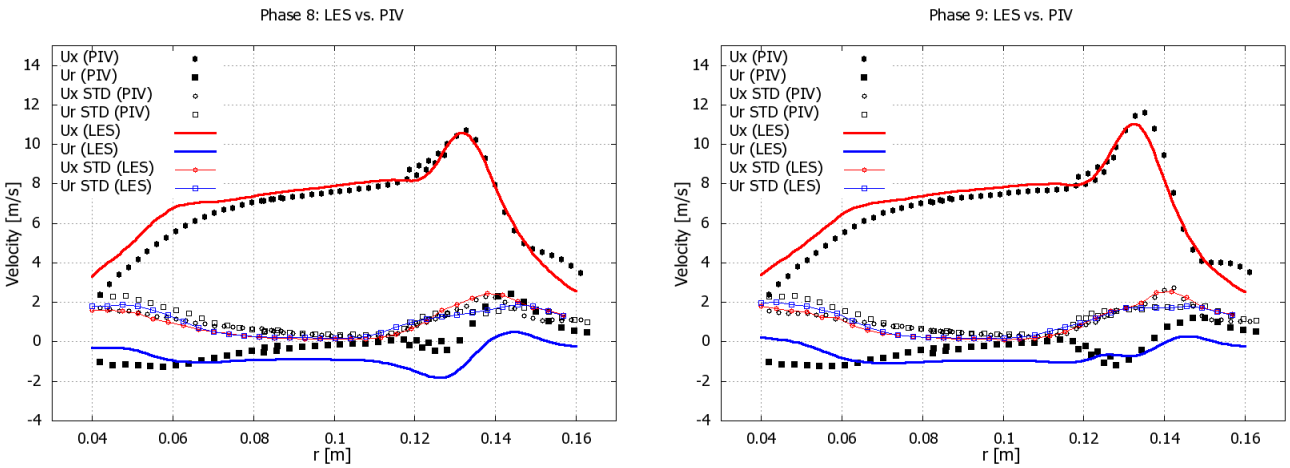

Figure 18: Comparison between LES and experimental measurements for phases 8 and 9.

Comparison between LES and experimental measurements

Overall, we found that LES predicted the gross parameters well: the pressure rise was 72 Pa vs. 75 Pa in experiment, and the shaft torque was predicted at 0.27 Nm vs. 0.29 Nm in experiment. We expect the quality of torque prediction to go up once the wall model is used.

For further code validation, we compare the mean and fluctuating components of axial and radial velocities at the prescribed location downstream, which was chosen to be 8 cm downstream of the back face of the fan hub. The result of this comparison is shown in Figures 14 through 18.

The LES prediction compares well with the experimental measurements, both in terms of mean and standard deviation of the velocity components. We consider the good match in the second-order statistics as an indicator that LES is able to predict well the small-scale structures of the flow, which are responsible for the broadband noise.

CONCLUSIONS

We have performed a Large Eddy Simulation of an engine cooling fan as a part of a larger effort in the area of computational noise prediction. To evaluate the quality of LES flow prediction we compared the results from the simulation to experimental measurements of pressure rise, shaft torque and PIV measurements for the flow velocities in the fan wake. The results show that LES captures the gross measurement parameters successfully as well as the mean and STD values of flow velocity components in the fan wake (although only one measurement location is mentioned in the paper, multiple locations in the fan wake were considered, all with comparable results).

Although the LES approach tends to be more computationally expensive than the industry-standard URANS, it has a distinct advantage of being able to capture the unsteady flow with high degree of fidelity, including energetic structures in the inertial range of turbulence that are responsible for the broadband component of the flow-borne noise.

We have not found the cost of the simulation to be overly prohibitive. This is in large part due to the good scalability of the LES code VIDA that we employ and also due to the advances in HPC speed and accessibility.

Overall we are confident that LES has a strong potential in the area of flow modeling for turbo-machinery, as well as to be a part of the noise prediction workflow during industrial product development process.

BIBLIOGRAPHY

[1] J Boudet, A Cahuzac, P Kausche, MC Jacob – *Zonal Large-Eddy Simulation of a Fan Tip-Clearance Flow, With Evidence of Vortex Wandering,* Journal of Turbomachinery 137, p. 061001, **2015**

[2] H Reese, C Kato, TH Carolus – *Large eddy simulation of acoustical sources in a low pressure axial-flow fan encountering highly turbulent inflow,* Trans ASME J Fluids Eng 129, p. 263, **2007**

[3] S Tomimatsu, Y Yamade, Y Hirokawa, N Nishikawa – *Prediction of flow field and aerodynamic noise of jet fan using large eddy simulation,* Journal of Visualization, 15, p.253-259, **2012**

[4] K Luo, S Zhang, Z Gao, J Wang, L Zhang, R Yuan, J Fan, K Gen – *Large –eddy simulation and wind-tunnel measurement of aerodynamics and aeroacoustics of a horizontal-axis wind turbine,* Renewable Energy 77, p0. 351-362, **2015**

[5] D Borello, A Corsini, G Delibra, M Fiorito – *Large-Eddy Simulation of a Tunnel Ventilation Fan,* Journal of Fluids Engineering, 135 p. 071102, **2013**

[6] S Bianchi, D Borello, A Corsini, F Rispoli, AG Sheard – *Large-Eddy Simulation of the Aerodynamics and Aeroacoustic Performance of a Ventilation Fan,* Advances in Acoustics and Vibration, Vol. 2013, Article ID 876973, **2013**

[7] M Wang, P Moin – *Computation of trailing-edge flow and noise using large-eddy simulation,* AIAA Journal, Vol. 38, No. 12, pp. 2201-2209, **2000**

[8] J Winkler, T Carolus, S Moreau – *Airfoil trailing-edge blowing: broadband noise prediction from large-eddy simulation,* APAA Paper 2009-3200, **2009**

[9] F. Ham – *An efficient scheme for large eddy simulation of low-Ma combustion in complex configurations,* CTR Annual Research Briefs 2007, Center for Turbulence Research, Stanford, p. 41, **2007**

[10] GA Brès, JW Nichols, SK Lele, FE Ham - *Unstructured Large Eddy Simulation of a hot supersonic over-expanded jet with chevrons,* AIAA Paper 2012-2213, **2012**

[11] A.W. Vreman – *An eddy-viscosity subgrid-scale model for turbulent shear flow: Algebraic theory and applications,* Physics of Fluids 16(10), p. 3670, **2004**

[12] J Smagorinsky – *General Circulation Experiments with the Primitive Equations I. The Basic Experiment,* Mon. Wea. Rev., 91(3), pp.99-164, **1963**

[13] M Germano, U Piomelli, P Moin – *A dynamic subgrid-scale viscosity model,* Phys. Fluids A, 3, p. 1760, **1991**

[14] M Shoeybi, M Svärd, F Ham, P Moin – *An adaptive implicit–explicit scheme for the DNS and LES of compressible flows on unstructured grids,* Journal of Computational Physics, 229, 5944–5965, **2010**

[15] K Sampath, J Katz – *Phase locked PIV measurements in wake of an automotive fan model.* FAN2015 Conference Proceedings (submitted), **2015**

[16] S Chumakov, YS. Shin, GA Bres, F Ham, J Nichols – *Noise prediction from a low-Mach number axial fan with LES and BEM.* FAN2015 Conference Proceedings (submitted), **2015**

[17] SK Godunov – *A difference method for numerical calculation of discontinuous solutions of the equation of hydrodynamics,* Matematicheskii Sbornik 89(3), p. 271-306, **1959**

[18] IJ Day – *The fundamentals of stall and surge,* Advances in Axial Compressor Aerodynamics (Lecture Series Monograph), von Karman Institute, Brussels, Belgium, **2006**

[19] M Inoue, M Kuroumaru, T Tanino, S Yoshida, M Furukawa – *Comparative studies on short and long length-scale stall cell propagating in axial compressor rotor,* ASME J. Turbomach., 123(1), p. 24, **2001**

[20] J März, C Hah, W Neise – *An experimental and numerical investigation into the mechanisms of rotating instability,* ASME J. of Turbomach., 124(3), p. 367, **2002**

[21] G Haller – *An objective definition of a vortex,* J. Fluid Mech., 525, p. 1-26, **2005**

[22] JC Hunt, A Wray, P Moin –*Eddies, stream, and convergence zone in turbulent flows,* Center for Turbulence Research report CTR-S88, **1988**

[23] J Jeong, F Hussain – *On the identification of a vortex,* J. Fluid Mech., 285, p. 69-94, **1995**